HLRZ2000-14
GUTPA/00/09/01
WUP-TH 00-17

Flavour singlet pseudoscalar masses in $N_f = 2$ QCD

T. Struckmann[a], K. Schilling[a,b]
G. Bali[c], N. Eicker[b] , S. Güsken[b], Th. Lippert[b],
H. Neff[a], B. Orth[b], W. Schroers[b], J. Viehoff[a], and P. Ueberholz[b]
[a] *NIC, Forschungszentrum Jülich, 52425 Jülich and DESY, 22603 Hamburg, Germany*
[b] *Fachbereich Physik, Bergische Universität, Gesamthochschule Wuppertal Gaußstraße 20, 42097 Wuppertal, Germany*
[c] *Department of Physics and Astronomy, The University of Glasgow, Glasgow G12 8QQ, Scotland*

(SESAM - TχL Collaboration)

We perform a lattice mass analysis in the flavour singlet pseudoscalar channel on the SESAM and TχL full QCD vacuum configurations, with 2 active flavours of dynamical Wilson fermions at $\beta = 5.6$. At our inverse lattice spacing, $a^{-1} \approx 2.3$ GeV, we retrieve by a chiral extrapolation to the physical light quark masses the value $m_{\eta'} = 3.7^{+8}_{-4} m_\pi$. A crude extrapolation from ($N_f = 3$) phenomenology would suggest $m_{\eta'} \approx 5.1 m_\pi$ for $N_f = 2$ QCD. We verify that the mass gap between the singlet state η' and the π flavour triplet state is due to gauge configurations with non-trivial topology.

I. INTRODUCTION

Lattice gauge theory (LGT) has been established as the standard method to deal with infrared aspects of quantum chromodynamics (QCD). Recently, the light hadronic flavour non-singlet masses have been accurately determined by $N_f = 2$ QCD simulations on the teracomputing scale [1]. Unfortunately, the situation is much less clear when it comes to the interesting physics of flavour symmetric hadronic states (like the η'-meson) which are expected to be influenced by the topological properties of the QCD vacuum: we have to await multi-teracomputing to see it settled.

The problem is due to the very occurrence of Zweig-rule forbidden contributions to the singlet hadronic propagator in form of disconnected diagrams, as already known from early feasibility studies in quenched QCD [2]. The difficulties arise for three reasons: (a) *eo ipso*, such disconnected correlators induce a high level of gauge field noise into the calculations; (b) their computation is costly as it involves momentum zero projections of quark loops, the evaluation of which requires the use of stochastic estimator techniques; (c) the propagator of a flavour singlet pseudoscalar meson, $C_{\eta'}$, turns out to be the *difference* between connected and disconnected diagrams with the possibility of numerical cancellations.

Indeed, at large Euclidean time separations, t, these cancellations are doomed to be strong if they are to render the large empirical flavour singlet/non-singlet mass gap [1], $M_0^2 \equiv M_{\eta'}^2 - M_\pi^2$. As a consequence, however, the signal-to-noise ratio becomes a serious problem for the direct lattice approach to flavour singlet objects and makes it hard to keep control on systematic errors. For all these reasons, *ab initio* full QCD lattice investigations of the η' mass have not yet overcome an exploratory stage. There is of course a way to avoid all this by following an indirect strategy and taking resort to the assumptions underlying the Witten-Veneziano formula [3]; this workaround amounts to determining the mass gap from *quenched* lattice determinations of the topological susceptibility [4].

Previous pioneering work in *full* QCD largely focussed on a two-step recipe to deal with the above problems: *(i)* determine m_π at large t and *(ii)* compute the mass gap [2], m_0, from the ratio of connected and disconnected correlators, $R(t) = C_{disc}(t)/C_{conn}(t)$ [5–7] in the range of smallish t-values. In our present approach we seek for a t-window within which a straightforward (one-step) flavour singlet propagator analysis can be pertinently achieved.

In a recent study we already applied improved stochastic estimator techniques — as geared previously for coping with disconnected operator insertions in the context of hadronic matrix elements [8] — on the flavour singlet correlators, with pointlike sources [9,10]. In this paper we shall show by a mass plateau analysis that a standard mass computation on the flavour singlet propagator itself will become feasible with reasonable control of systematic errors, once smeared operators are used.

[1] In our $N_f = 2$ world we have a triplet (rather than an octet) of flavour non-singlet mesons. Moreover, working with mass-degenerate quarks, our π's are exactly mass degenerate too.

[2] Upper (lower) case letters refer to masses in physical (lattice) units.

II. LATTICE PREREQUISITES

We consider the pseudoscalar flavour singlet operator in a flavour symmetric theory

$$S(x) = \sum_{i=1}^{N_f} \overline{q}_i(x)\gamma_5 q_i(x) \ , \tag{1}$$

with N_f flavours. By the usual Wick contraction it leads to the flavour singlet propagator in terms of the inverse Dirac operator, $\Delta \equiv D^{-1}$:

$$\begin{aligned} C_{\eta'}(0|x) \sim \langle & N_f \mathrm{tr}(\Delta(0|x)\Delta^\dagger(0|x)) \\ & -N_f^2 \mathrm{tr}(\gamma_5\Delta^\dagger(0|0))\mathrm{tr}(\gamma_5\Delta(x|x))\rangle \ , \end{aligned} \tag{2}$$

which is a sum of fermionic connected and disconnected contributions with traces to be taken in the spin and colour spaces. In the rest of the paper we shall refer to them as 'one-loop' and 'two-loop' contributions, respectively. The traces are computed with Z_2 noise sources including diagonal improvement as explained in ref. [9].

The momentum zero projection

$$C_{\eta'}(t) \equiv \langle S(t)S(0)\rangle_{conn} - \langle S(t)S(0)\rangle_{disc} \tag{3}$$

is expected to decay exponentially, $\sim \exp(-m_{\eta'}t)$, and thus to reveal the flavour singlet mass, $m_{\eta'}$. On a toroidal lattice with temporal extent T one should encounter the usual cosh behaviour at large values of t and $T-t$

$$C_{\eta'}(t) \to \exp(-m_{\eta'}t) + \exp(-m_{\eta'}(T-t)) \ . \tag{4}$$

From this parametrization effective masses, $m^t_{\eta'}$, can be retrieved by solving the implicit equations

$$\frac{C_{\eta'}(t+1)}{C_{\eta'}(t)} = \frac{\exp(-m^t_{\eta'}(t+1)) + \exp(-m^t_{\eta'}(T-t-1))}{\exp(-m^t_{\eta'}t) + \exp(-m^t_{\eta'}(T-t))} \ . \tag{5}$$

For sufficiently large values of t, the effective masses should saturate into a plateau. The crucial question is, however, whether one can establish a *t-window of observation* that reveals a definite plateau behaviour of $m^t_{\eta'}$ before noise takes over.

A. Operator smearing

The building blocks for hadronic observables are the quark propagators, ξ, which may be computed by solving the (discretized) Dirac equation with appropriate source vectors, $\phi_s(z)$, on the lattice:

$$D(z,x)\xi(x) = \phi_s(z) \ . \tag{6}$$

In standard spectrum analysis one generally applies some kind of spatial smearing to the hadron source (located at $t=0$) in order to enhance the ground state signals of the resulting hadronic operators at medium values of t. Needless to say, this appears to be all the more necessary in the present context where – as explained above – we are faced both with (a) cancellations (between C_{conn} and C_{disc}) and (b) noisier signals (from C_{disc}).

We used our smearing procedure as applied in the analysis of light non-singlet masses [11]; it is characterized by N diffusive iteration steps

$$\phi_s^{(i+1)}(x) = \frac{1}{1+6\alpha}\left[\phi_s^{(i)}(x,t) + \alpha\sum_\mu \phi_s^{(i)}(x+\mu)^{\mathrm{p.t.}}\right] \ , \tag{7}$$

where the index 'p.t.' stands for 'parallel transported', and the sum extends over the six spatial neighbours of x. For $\phi_s^{(0)}$ we start out from pointlike sources for the connected and Z_2-noise nonlocal sources for the disconnected diagrams. In this way the bilinear quark operators, Eq. (1), were computed after $N=25$ such smearing steps, with the value $\alpha = 4.0$. The smearing procedure was applied to meson sources as well as to sinks – both for C_{disc} and C_{conn}, in order to correctly maintain their relative normalisations.

TABLE I. Simulation parameters used at $\beta = 5.6$ and numbers of stochastic sources (used with local and smeared operators, N^{ll}_{est}, N^{sm}_{est}). Last column: numbers of available decorrelated vacuum field configurations, N_{conf}.

κ_{sea}	m_π/m_ρ	L^3*T	N^{ll}_{est}	N^{sm}_{est}	N_{conf}
0.1560	0.834(3)	16^3*32	400	400	195
0.1565	0.813(9)	16^3*32	400	400	195
0.1570	0.763(6)	16^3*32	400	400	195
0.1575	0.692(10)	16^3*32	400	400	195
0.1575	0.704(5)	24^3*40	400	100	156
0.1580	0.574(13)	24^3*40	100	100	156

In table I we list the run parameters of our simulations, which make use of vacuum field configurations generated by the SESAM ($16^3\times 32$ lattice [12]) and the TχL ($24^3\times 40$ lattice [13]) collaborations, both with $N_f=2$ and $\beta = 5.6$. We have used five different sea quark masses and two different lattice sizes to gain some control on finite-size effects. While the number of vacuum configurations varies from 156 to 195, the number of independent stochastic sources has been chosen to be 400 on the small lattices, both for local (ll) and smeared (sm) operators. On the large lattices 100 (400 for $\kappa_{sea} = 0.1575$-ll) source vectors were used.

Fig. 1 illustrates the quality of our data in terms of the one-loop and two-loop correlators at the lightest sea quark mass on the SESAM lattice, computed with pointlike (upper figure) and smeared operators (lower figure), using $N_{est} = 400$ stochastic Z_2-noise sources with diagonal improvement [9]. The errors quoted are statistical and have been obtained by jackknifing. We find a marked improvement of the signal by help of source smearing in the regime $5 \le t \le 12$.

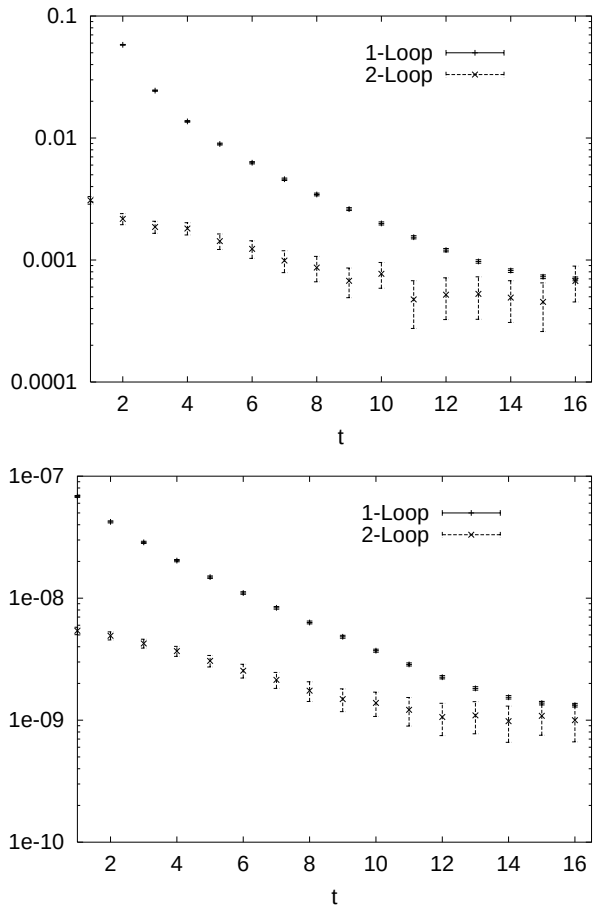

FIG. 1. Effect of smearing on the correlation functions. SESAM configurations at the lightest sea quark mass, $\kappa_{sea} = 0.1575$. Top figure: local operator; bottom figure: smeared operator. Upper (lower) data set refers to one-loop (two-loop) contributions.

One should remember that the data points in Fig. 1 suffer from two kinds of stochastic noise: the one from the gauge fields and the one from the noisy sources. In order to disentangle them it is highly instructive to study the error on the two-loop signal, σ, as a function of the number of stochastic sources, N_{est} . In Fig. 2 we plot this quantity for the SESAM ensemble at $\kappa_{sea} = 0.1570$ on a time slice of interest, $t = 8$. At sufficiently large values of N_{est} the parametrization

$$\sigma^2 = \frac{\Sigma^2_{est}}{N_{est}} + \Sigma^2_{conf} \qquad (8)$$

is expected to describe the superposition of errors from source and gauge field fluctuations. Therefore, the error analysis can provide a useful check on the quality of the stochastic estimator outputs. The data in Fig. 2 indeed yield convincing evidence for early asymptotic N_{est}-dependence, with a threshold value $N_{est} \simeq 64$. Moreover, we find that on the SESAM sample the genuine gauge field noise (as indicated by the horizontal asymptotic $N_{est} \to \infty$ line) prevails once we choose $N_{est} \geq 100$. As to the subasymptotic regime, one might attribute the apparent 'non-standard' behaviour of σ to pollutions from subleading, non-trace terms in the stochastic estimate of the loops.

The main message from Fig. 2 is that the Z_2 noise method does provide reasonable parametric control over the additional fluctuations induced by the stochastic estimator on the observable. This control cannot be taken

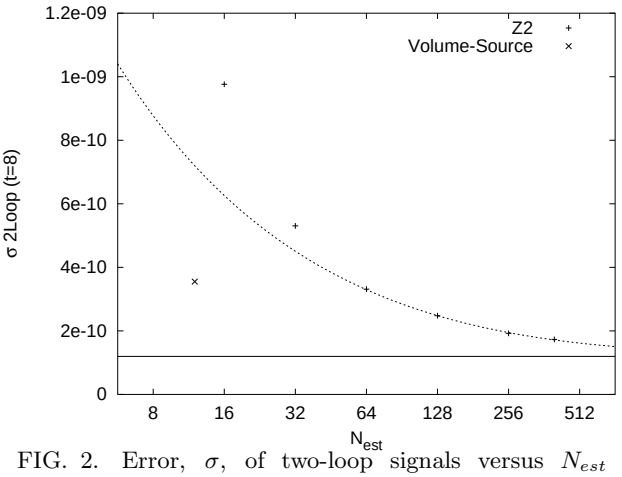

FIG. 2. Error, σ, of two-loop signals versus N_{est} at $\kappa_{sea} = 0.1570$ on time slice $t = 8$, for smeared sources and sinks. The curve is the best fit according to the parametrisation given by Eq. (8).

for granted when applying the volume source technique (12 color-spin explicit inversions per configuration) which refrains from using stochastic sources and relies fully on gauge invariance and gauge noise for the suppression of nondiagonal contributions to the trace estimates [2]. For comparison, however, we have included the corresponding error as we computed it on our gauge field ensemble.

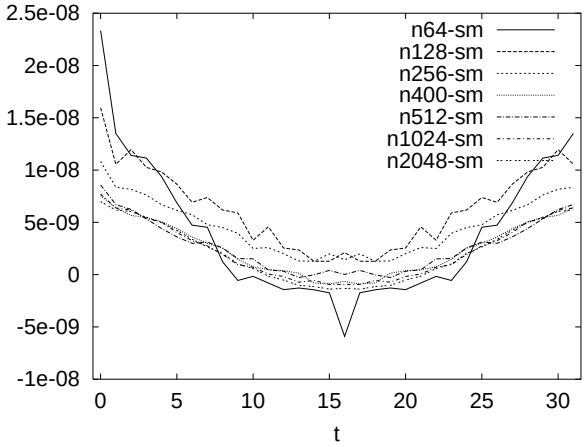

FIG. 3. t-dependence of the two-loop signal, on a single configuration with smeared operator, for various values of N_{est}.

Complementary to these considerations one may study

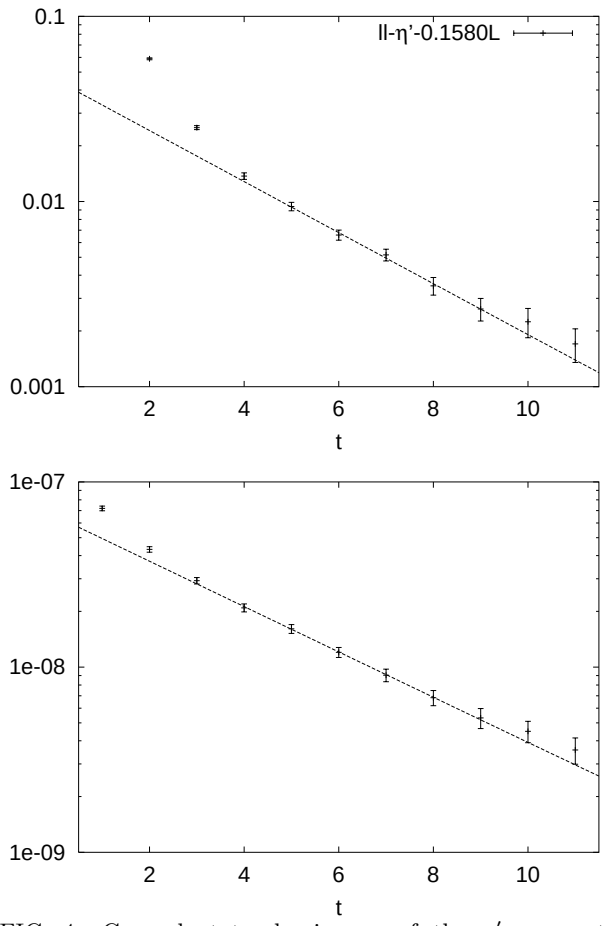

FIG. 4. Ground state dominance of the η'-propagator ($\kappa_{sea} = 0.1580$), with smeared sources and sinks. Top: with local operators, bottom: with smeared operators.

the overall (in t) effects of finite source sampling on the estimate of the two-loop correlator for a particular gauge configuration. Fig. 3 illustrates, again at $\kappa_{sea} = 0.1570$ on the small lattice, the kind of fluctuations induced by the stochastic sources of the two-loop correlator with smeared operators at various values of N_{est} which we ran up to 2048 in this case. It appears that on our sample the Z_2 noise injected from the sources into the correlator is adequately suppressed at $N_{est} \approx 400$. This justifies again that on the small lattices $N_{est} = 400$ is a reasonable choice for the present study. On the large lattices, however, enhanced self-averaging effects allow for a smaller number of stochastic sources, $N_{est} \simeq 100$.

We are now in the position to study plateau formation on our ensemble of vacuum configurations.

B. Plateaus of effective masses from smearing

The effect of smearing on the flavour symmetric correlator, $C_{\eta'}$, is visualized in the comparative twin plot of Fig. 4, as obtained at our smallest quark mass on the TχL lattice. *Prima vista* we do find reasonable signals on this correlator up to $t \approx 10$. Moreover, by inspection of the cosh-fits, we find a considerable decrease of excited state contributions as a result of smearing.

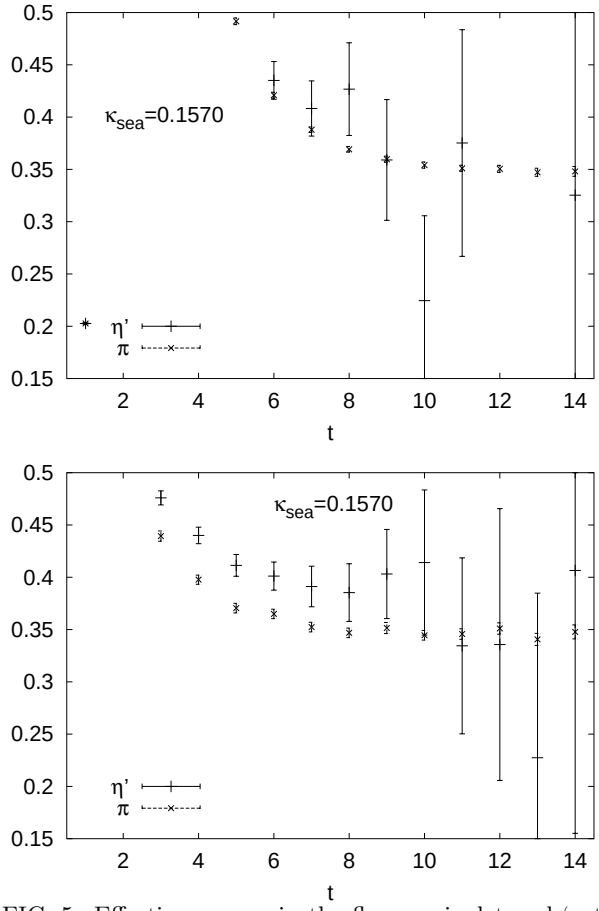

FIG. 5. Effective masses in the flavour singlet and 'octet' channels, with pointlike (top) and smeared operators (bottom), at $\kappa_{sea} = 0.1570$.

Let us now scrutinize the situation by turning to the analysis of effective masses as extracted from Eq. (5). We have seen in ref. [9] that, given our sample sizes, the use of local sources and sinks does not provide sufficient resolution to reveal such plateau formation in the effective flavour singlet mass plots. This situation is illustrated in Fig. 5 where we confront, at a particular intermediate

TABLE II. Fit ranges

κ_{sea}	$L^3 * T$	π-ll-Fit	η'-ll-Fit	π-sm-Fit	η'-sm-Fit
0.1560	$16^3 * 32$	$12-16$	$6-9$	$9-16$	$5-10$
0.1565	$16^3 * 32$	$13-16$	$6-9$	$9-16$	$5-10$
0.1570	$16^3 * 32$	$12-15$	$6-9$	$9-16$	$5-10$
0.1575	$16^3 * 32$	$12-15$	$6-9$	$9-16$	$6-11$
0.1575	$24^3 * 40$	$12-15$	$6-9$	$9-16$	$5-9$
0.1580	$24^3 * 40$	$12-15$	$6-9$	$9-16$	$5-9$

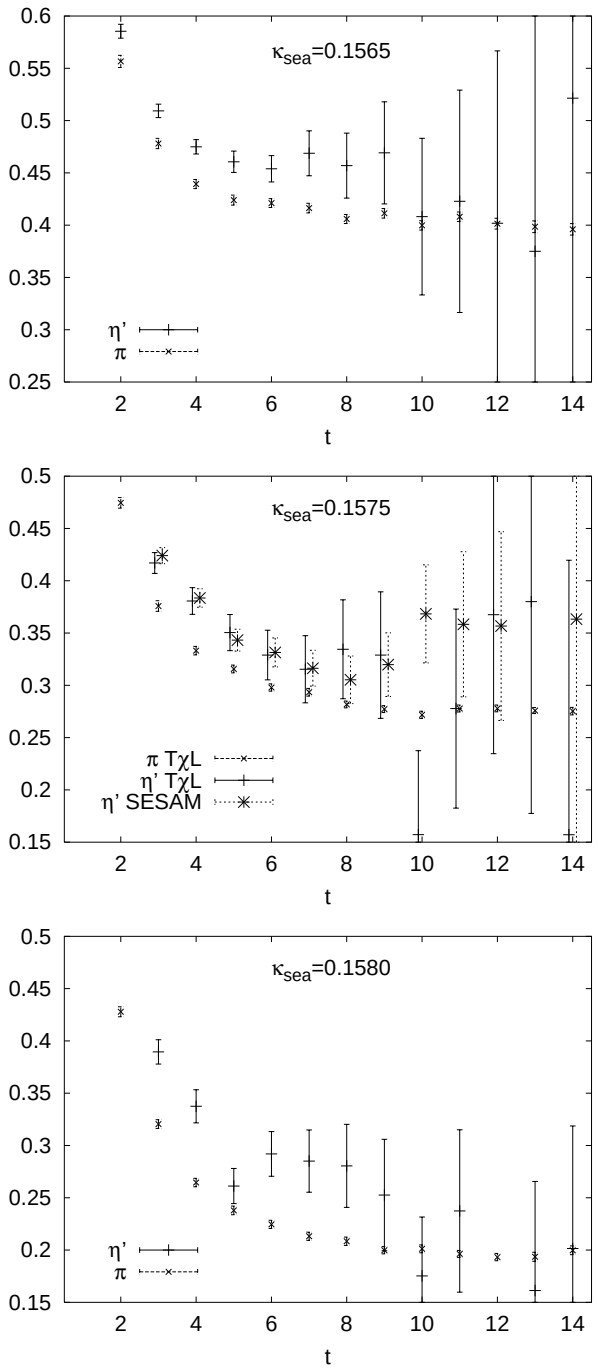

FIG. 6. Plateau formation in the effective η'- and π masses with smeared operators at various sea quark masses. At $\kappa_{sea} = 0.1575$, η'-results from SESAM and TχL configurations are plotted separately.

sea quark mass ($\kappa_{sea} = 0.1570$), effective pseudoscalar masses obtained both with and without operator smearing. Obviously, with pointlike operators, one has to resort to *bona fide* single cosh fits on the correlators without any kind of systematic error control on the extracted flavour singlet 'masses'. After source and sink smearing, however, our data begins to reveal plateau formation in

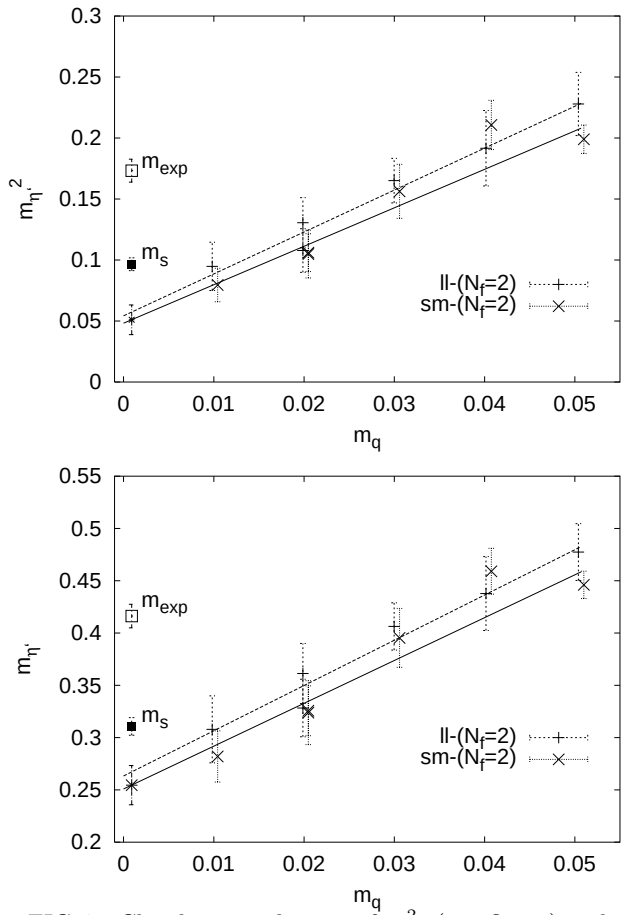

FIG. 7. Chiral extrapolations of $m^2_{\eta'}$ (top figure) and $m_{\eta'}$ linear in quark mass.

the singlet channel.

In Fig. 6 we display the evidence for plateau formation through operator smearing for the remaining sea quark masses in the range $0.1565 \leq \kappa_{sea} \leq 0.1580$. Here again the 'octet' channel masses are included for reference in order to enable judgement on the sensitivity for mass gap determinations. We emphasize again that all singlet data are obtained after symmetric source *and* sink smearing, as described above. It appears that smearing meets the expectation by increasing the ground state overlap: this opens the window of observation for a mass plateau from $t = 5$ onwards where statistical errors are still 'tolerable'. By comparing the SESAM and TχL data sets at $\kappa_{sea} = 0.1575$ we find no evidence for a volume effect on $m_{\eta'}$ [14].

III. PHYSICS ANALYSIS

Encouraged by the apparent plateau formation we proceed next to carry out mass fits based on a *single* cosh ansatz, with t-ranges as listed in table II. For reference we have also included information about the fit-ranges previously used with local sources [9].

A. Chiral extrapolations

Because of the well-known technical limitations of the hybrid Monte Carlo algorithm [15] the SESAM and TχL configurations correspond to two mass-degenerate light sea quark flavours ($N_f = 2$), with the unrenormalized mass value

$$m_q = M_q a = 1/2(\kappa^{-1} - \kappa_c^{-1}) \; . \tag{9}$$

From our previous light spectrum analysis [11] we quote the lattice spacing

$$a_\rho^{-1}(\kappa_{light}) = 2.302(64)\mathrm{GeV} \tag{10}$$

and the critical and physical light quark κ values:

$$\kappa_c = 0.158507(44) \quad , \quad \kappa_{light} = 0.158462(42) \; . \tag{11}$$

Our data do not allow to decide whether it is $m^2_{\eta'}$ or $m_{\eta'}$ that follows a linear quark mass dependence: as shown in Fig. 7, both ansätze render $\chi^2/d.o.f. \simeq \mathcal{O}(1)$. We emphasize in this context that we make *no distinction* between sea and valence quarks as we choose the quark masses in the fermion loops to equal the sea quark masses (symmetric extrapolation in the sense of ref. [11]).

We display the results on the η' mass and the mass gap

$$m_0^2 = m^2_{\eta'} - m^2_\pi \; , \tag{12}$$

for both forms of extrapolation in table III. For comparison, we have also included previous estimates as obtained by using local sources [9].

B. Comparison to experiment

In the $N_f = 2$ world of our simulations, according to Eq. (2), we would not expect to encounter the full effect of Zweig rule forbidden diagrams, and hence we anticipate to underestimate the real world η' mass, $m_{\rm exp}$, (plotted as open squares in Fig. 7).

From the experimental mass splitting

$$M^2_{0,n_F=3} \equiv M^2_{\eta',n_F=3} - M_8^2, \quad M_8^2 \equiv 2M_K^2 - M_\eta^2 \; , \tag{13}$$

we therefore compute, in the spirit of the Witten-Veneziano formula,

TABLE III. η' and m_0 results

Ensemble	Fit	$m_{\eta'}$	m_0	$M_{\eta'}$ [MeV]	M_0 [MeV]
$N_f = 2$	m-ll	.267(23)	.251(43)	615(53)	576(99)
$N_f = 2$	m^2-ll	.239(37)	.245(40)	551(85)	565(92)
$N_f = 2$	m-sm	.255(19)	.205(43)	587(44)	472(99)
$N_f = 2$	m^2-sm	.226(25)	.222(26)	520(58)	510(62)

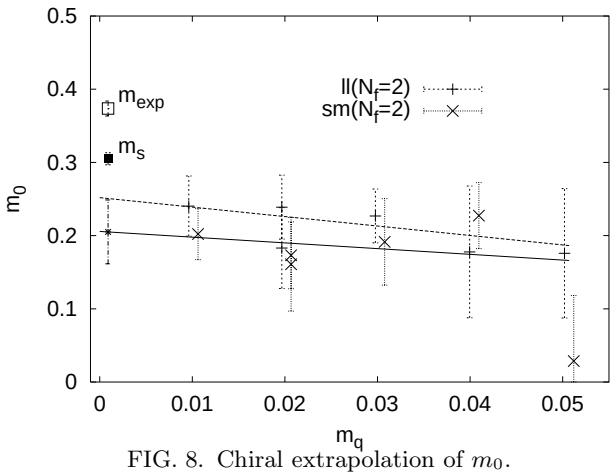

FIG. 8. Chiral extrapolation of m_0.

$$M_0^2 = 2N_f \chi_q / F_\pi^2 \; , \tag{14}$$

the 'pseudoexperimental' value, M_s, in our $N_f = 2$ world:

$$M_s^2 = 2/3\, M^2_{0,n_F=3} + M_\pi^2 = (715\ \mathrm{MeV})^2 \; . \tag{15}$$

This value corresponds in lattice units to the full squares marked 'm_s' in the two alternative chiral extrapolations shown in Fig. 7. Let us compare this latter value with the lattice $N_f = 2$-prediction in terms of numbers: when we set the scale by the ρ mass, the extrapolation of $m^2_{\eta'}$ to the physical quark mass yields the value

$$M^2_{\eta'} = (520^{+125}_{-58}\mathrm{MeV})^2 \tag{16}$$

at our lattice spacing. We have linearly added the difference between the two extrapolations (of $m_{\eta'}$ and $m^2_{\eta'}$) to the statistical error to accomodate systematic uncertainties. The difference between this value and the 715 MeV of Eq. (15) may be attributed to finite-a effects. For comparison, we also performed a linear extrapolation of the mass splitting, m_0, as given in Eq. (12) which shows only little quark mass dependency (see Fig. 8). This is

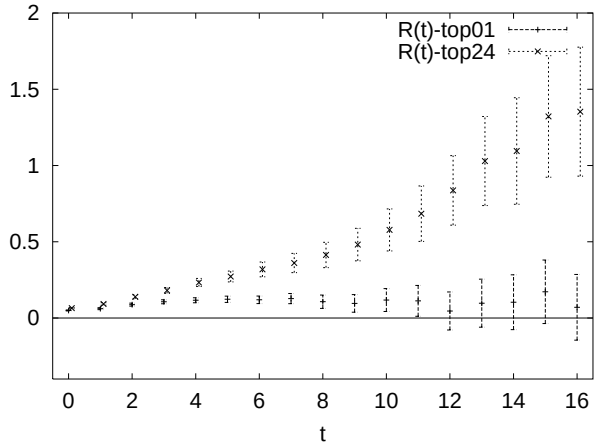

FIG. 9. Ratio of C_{disc}/C_{conn} for $\kappa_{sea} = .1575$ (top figure) with cuts in topological charge as explained in the text.

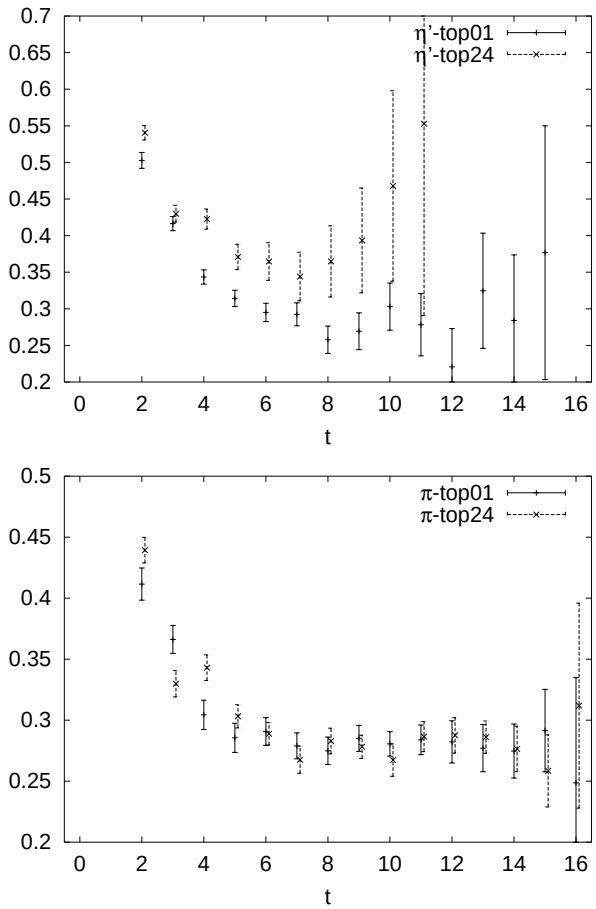

FIG. 10. Effective η' (top) and π (bottom) masses for $\kappa_{sea} = .1575$, with cuts in topological charge as explained in the text.

consistent with the weak dependence of F_π on the quark mass observed on SESAM configurations [11]. From the value $F_\pi = 116(8)$ MeV obtained for $N_F = 2$ QCD at our lattice spacing and Eq. (16) we obtain the estimate $\chi_q = (170^{+27}_{-15}\,\mathrm{MeV})^4$ for the quenched topological susceptibility of Eq. (14), which is consistent with the value 180 MeV from 3 flavour phenomenology [3].

C. Impact of topology

The Witten-Veneziano mass formula, Eq. (14), relates the difference between the η' mass and the flavour non-singlet pseudoscalar mass to the topological susceptibility χ_q of the *quenched* gauge vacuum. This scenario motivates us to investigate in *full* QCD whether the ratio $R_Q(t) = C_{disc}(t)_Q / C_{conn}(t)_Q$, whose deviations from zero give rise to the observed mass gap, is correlated with $|Q|$, the modulus of the topological charge, configuration by configuration. If we restricted our analysis for instance to gauge configurations with $Q = 0$ only, the topological susceptibility, $\chi = \langle Q^2 \rangle / V$, determined on this subensemble, would vanish as well and we might expect the π to be mass degenerate with the η'. On the other hand, if we rejected configurations with small $|Q|$-values, the effective χ on the remaining sample would be enhanced and the generated mass gap increased.

In Fig. 9 we show, for $\kappa_{sea} = 0.1575$ and the small lattice, the quantity $R_Q(t)$ with cuts applied according to $|Q| \leq 1.5$ (top01) and $|Q| > 1.5$ (top24), the topological charge being determined as in ref. [16]. The value of 1.5 was chosen such as to obtain two ensembles *of comparable statistics* in topologically different vacuum sectors. We do find a definite dependence of R_Q on $|Q|$. Note in particular that the disconnected piece vanishes in the vacuum sector with small values of $|Q|$! This feature reflects itself of course in the corresponding effective masses of the flavour singlet and non-singlet mesons. This is shown in Fig. 10: the restricted flavour singlet mass, $m_{\eta'}|_{|Q|\leq 1.5}$, turns out to be identical to the 'octet' meson mass $m_3 = m_\pi$. Accordingly, the flavour singlet-non-singlet mass gap is due to nontrivial topological vacuum structures.

On the other hand, the 'octet' meson mass appears to be not at all sensitive to such restrictions to topological sectors; this seems to be a general feature of flavour non-singlet light hadron spectrum observables [17].

IV. SUMMARY AND CONCLUSIONS

Using smeared operators and reasonable source statistics on the SESAM and TχL samples of QCD vacuum configurations we found clear indications of plateau formation in the effective flavour singlet pseudoscalar mass plot in the intermediate t-regime. The η' mass is definitely sensitive to the topological structure of the QCD vacuum. In our two-flavour simulation its actual value after chiral extrapolation turns out to be in qualitative agreement with the expectation from experiment, but further studies are needed to pin down finite-a effects.

At this stage the statistical errors on the singlet masses are mostly due to gauge field fluctations and by a factor $\simeq 5$ larger than for the non-singlet ones. Clearly, the next generation teracomputers will open the door to go for lattice determinations of Zweig-rule forbidden objects with an accuracy known so far only from light non-singlet hadron spectroscopy.

In the meantime we are working on computational techniques to determine quark loops in the regime of quark masses lighter than attained so far [18].

ACKNOWLEDGMENTS

We enjoyed interesting discussions with John Negele. TS thanks Thorsten Feldmann for fruitful conversations. BO, TS, and WS appreciate support from the DFG Graduiertenkolleg "Feldtheoretische und Numerische Methoden in der Statistischen und Elemen-

tarteilchenphysik". Our European collaboration was funded by the EU network "Hadron Phenomenology from Lattice QCD" (HPRN-CT-2000-00145). GB has been supported by EU grant HPMF-CT-1999-00353. The HMC productions were run on APE100 systems at INFN Roma and at NIC Zeuthen. We are grateful to our colleagues F. Rapuano and G. Martinelli for the fruitful TχL -collaboration. Analysis was performed on APE100 and CRAY T3E systems at NIC and the University of Bielefeld.

---

[1] A. Ali Khan *et al* , [CP-PACS - Collaboration] , *Nucl. Phys. Proc. Suppl.* B **83**, 176 (2000); *Dynamical quark effects on light quark masses*, hep-lat/0004010.
[2] Y. Kuramashi *et al* , *Phys. Rev. Lett.* **72**, 3448 (1994).
[3] E. Witten, *Nucl. Phys.* B **156**, 269 (1979); G. Veneziano, *Nucl. Phys.* B **159**, 213 (1979).
[4] P. DiVecchia *et al* , *Nucl. Phys.* B **192**, 392 (1981); J. Hoek *et al* , *Nucl. Phys.* B **288**, 589 (1987); M. Campostrini *et al* , *Phys. Lett.* B **252**, 436 (1990).
[5] G. Kilcup *et al* , *Nucl. Phys. Proc. Suppl.* B **47**, 358 (1996); L. Venkatamaran *et al* , *Nucl. Phys. Proc. Suppl.* B **53**, 259 (1997) and hep-lat/9711006.
[6] A. AliKhan *et al* , [CP-PACS - Collaboration], *Nucl. Phys. Proc. Suppl.* B **83-84**, 162 (2000), hep-lat/9909045.
[7] Ch. Michael *et al* , [UKQCD - Collaboration], *Nucl. Phys. Proc. Suppl.* B83-841852000, C. McNeile and C. Michael, [UKQCD - Collaboration] *The η and η' mesons in QCD*, hep-lat/0006020.
[8] J. Viehoff *et al* , [SESAM - Collaboration], *Nucl. Phys. Proc. Suppl.* B **63**, 269 (1998); *Nucl. Phys. Proc. Suppl.* B **73**, 856 (1999); J. Viehoff, DESY-THESIS-1999-036, WUB-DI-1999-17, Sept. 1999, 94pp.
[9] T. Struckmann *et al* , [SESAM - Collaboration], *Probing the QCD vacuum with flavor singlet objects: η' on the lattice*, hep-lat/0006012.
[10] T. Struckmann, DESY-THESIS-2000-, WUB-DI-2000-5.
[11] N. Eicker *et al* , [SESAM - Collaboration], *Phys. Rev.* D **59**, 14509 (1999).
[12] Th. Lippert *et al* , [SESAM - Collaboration], *Nucl. Phys. Proc. Suppl.* A **60**, 311 (1998).
[13] L. Conti *et al* , [TχL - Collaboration], *Nucl. Phys. Proc. Suppl.* B **53**, 222 (1997).
[14] for volume effects in the flavour non-singlet spectrum, see B. Orth *et al* , [SESAM - Collaboration], in preparation.
[15] see e.g. the review of A.D. Kennedy, Parallel Computing **25** 1311 (1999).
[16] B. Alles *et al* , [SESAM - Collaboration], *Phys. Rev.* D **58**, 071503 (1998); Th. Lippert *et al* , [SESAM - Collaboration], *Nucl. Phys. Proc. Suppl.* B **73**, 521 (1999).
[17] G. Bali *et al* , [SESAM - Collaboration], in preparation.
[18] H. Neff *et al* , [SESAM - Collaboration], work in progress.